A method of characteristics for solving population balance equations (PBE) describing the adsorption of impurities during crystallization processes

François Févotte, Gilles Févotte

A method of characteristics for solving Population Balance Equations (PBE) describing the adsorption of impurities during crystallization processes.

François Févotte[*] and Gilles Févotte[1]**

** 99, Avenue de Verdun. 92130 Issy les Moulineaux (France)*

*** Ecole des Mines de Saint Etienne, Centre SPIN. 158, Cours Fauriel. 42000 Saint Etienne & Université Lyon 1, 43, Avenue A. Einstein, 69622 Villeurbanne, Cedex (France).*

fevotte@emse.fr

Abstract: Possible hindering effects of impurities on the crystal growth were shown to take place through the adsorption of impurity species on the crystal surface. Transient features of this adsorption were also observed, such that the growth of a given crystal does not depend on supersaturation only, but also on the time a given particle spent in contact with impurities present in the mother liquor. Meanwhile, few kinetic models describe the effect of impurities on the growth of crystals in solution, and published models are usually derived from data obtained thanks to specific experiments based on the evaluation of the growth rate of singles crystals. Such models are obviously questionable because, in the industrial practice, distributed properties of crystals are actually involved. Considering the "time of contamination" of particles as a new internal variable is thus made necessary. This is the reason why a specific PBE resolution algorithm is presented in this paper. The numerical scheme for the resolution of PBEs is based on the method of characteristics and shown to allow fast and accurate simulation of transient features of the crystal size distribution in the particular case when the growth or nucleation rates are assumed to exhibit unsteady-state dynamics. Thanks to this algorithm and through the simulation of isothermal seeded desupersaturation crystallization operations of citric acid, important industrial features of crystallization in impure media are satisfactorily reproduced.

Keywords. Crystallization, Dynamic simulation, Nucleation, Population balance, Particulate processes, Impurities.

[1] To whom correspondence should be addressed

1. INTRODUCTION

1.1 Impurities in solution crystallization.

Actually, almost all modelling and control papers in the field of crystallization deal with pure solute/solvent systems, which is obviously a very significant limitation because it is well known that industrial crystallization processes cannot avoid undesirable impurities to be generated during the many chemical reactions preceding the crystallization steps. Even minute concentrations of impurities present in the initial solution can affect tremendously the crystallization process (Sangwal, 1996; Wood, 2001; Myerson, 2001; Chernov, 2004; Sangwal, 2007) and induce significant reductions of the growth rate (Sangwal, 1996; Kubota et al., 2000; Kubota, 2001).

As far as the advanced dynamic modelling of crystallization systems is concerned, and to the best of our knowledge, such key-features of "real" industrial crystallization processes (i.e. processes performed in the unavoidable presence of impurities) have never been described using PBEs so that one cannot evaluate the distribution and the time-variations of the detrimental effects of impurities during crystallization processes.

From an industrial point of view, obvious unwanted consequences of impurities in crystallizing media have therefore to be dealt with:

- Due to final intractable residual supersaturation, the yield of the crystallization operation is reduced because the solubility equilibrium can no more be reached.

- Undesirable growth rates reductions require increasing the duration of the crystallization operation, and therefore reduce the process productivity.

- As impurities can incorporate the crystal lattice, controlling the final chemical purity of the particles is obviously a major quality issue. In the field of pharmaceutical production for example (see e.g. Chow et al. 1985; Johnson & Li, 2007; Raghavan et al. 2001), it is clear that for the sake of public health, the concentration of harmful impurity species in final active ingredients is strictly controlled by public regulatory agencies such as the US FDA (Federal Drug Administration).

It is the goal of the present paper to address this problem, and to present a new numerical scheme allowing one to solve the related PBEs.

1.2. Population Balance Equations (PBE) and crystallization

PBEs are widely used as a modeling tool in the engineering of dispersed media, with applications including crystallization, powder technologies, polymerization processes, biotechnologies, etc (see e.g. Mersmann et al., 2002; Ramkrishna 2000, Ramkrhisna and Mahoney, 2002, Vale & Mc Kenna, 2005; Liao & Lucas, 2009).

In the monodimensional size case, the PBE reduces to the well-known following partial differential equation allowing one to compute the time variations of the Crystal Size Distribution (CSD). For the sake of simplicity, supersaturation σ is omitted in the list of arguments, even though it is the driving force of almost all crystallization phenomena:

$$\begin{cases} \dfrac{\partial \psi(L,t)}{\partial t} + G(t)\dfrac{\partial \psi(L,t)}{\partial L} = 0 & (1) \\ \psi(L,0) = 0 \quad or \quad \psi(L,0) = \psi_{seed} & (2) \\ \psi(0,t) \cong \psi(L^*,t) = \dfrac{R_N(t)}{G(t)} & (3) \end{cases}$$

The initial condition (2) accounts for the possibility of the crystallization to start through primary nucleation (i.e. no solid phase is initially present in the crystallizer) or through seeding, which consists in the introduction of small amounts of particles, usually sieved, in the supersaturated solution. Due to the supersaturated state of the solution, seed particles initiate the crystallization process and are characterized by their size distribution ψ_{seed}.

R_N is the rate of nucleation expressed in #.s^{-1}.m^{-3}.

$G = \dfrac{dL}{dt}$ is the crystal growth rate, in m.s^{-1}, which is likely to be affected by the presence of impurities, as explained in more details in the next Part.

Many systems exist where impurities were shown to lead to supersaturation thresholds below which the development of crystallization is fully inhibited (see e.g. Sangwal, 2002). To the best of our knowledge, such key-features of “real” industrial crystallization processes (i.e. processes performed in the unavoidable presence of impurities) were never described using PBEs.

Now, from a more technical point of view, if one considers the variety of the techniques which were proposed to solve the PBEs in the case of crystallization processes, it appears that few of these methods are based on the method of characteristics (MOC). It is however known that MOCs avoid numerical diffusion errors and oscillatory solutions caused by the discretization of the involved growth term, especially when steep or discontinuous particulate phenomena take place in suspension (Kumar and Ramkrishna, 1997; Briesen, 2006). Qamar and Warnecke (2007) have proposed a numerical method for solving PBEs involving nucleation, growth and aggregation processes. The scheme combines a method of characteristics for computing the growth term with a finite volume technique for calculating aggregation terms. The method is compared to a finite volume method through the modelling of "academic" situations for which analytical solutions are available. The numerical scheme based on MOC is shown to be more efficient than pure finite volume schemes. This interesting feature of MOC is attributed to the semi-analytical integration of the advection term $\partial G\psi/\partial L$ from the main PBE. Sotowa *et al.* (2000) compare the numerical resolution of a simple crystallization PBE using a finite difference method and the method of characteristics to evaluate the impact of numerical dispersion on the design of feedback controllers. It is finally concluded that, as far as the simulation of control systems is concerned, the method of characteristics is recommended for simulating crystallization processes. More recently, in order to simulate the growth of anisotropic particles, Briesen (2006) proposed a reduced two-dimensionnal PBE model. Here, the MOC approach was used to validate the calculations.

It is the goal of the present paper to address the problem of accounting for the "birthdate" of crystals in the governing crystallization PBE, and to propose a new numerical scheme, based on MOC, for the resolution of the latter PBE. In fact, it is clear that the approach proposed by Kumar and Ramkrishna (1996a-b, 1997) in their series of three papers is much more "advanced" than the approach presented here, both in terms of the accuracy of the used size integration technique and with respect to the ability of the technique to describe agglomeration and breakage phenomena. Nevertheless, the present algorithm offers another way of considering nucleation phenomena and, through its great simplicity, can be valuable for applications where fast computation is required (e.g. for in-line feedback control applications or for kinetic parameter estimation).

1.3. Crystal growth rate.

In most published crystallization PBE modeling works the crystal growth rate G is assumed not to depend on the particle size (McCabe's hypothesis), but essentially on supersaturation. Several expressions of the supersaturation may actually be used, according to the theoretical background of the study. The following equations define the relative supersaturation $\sigma(t)$ and the supersaturation ratio $\beta(t)$, which both are adimensional variables:

$$\sigma(t) = \frac{C(t) - C^*}{C^*} \quad (4)$$

$$\beta(t) = C(t)/C^* \quad (5)$$

$$\Delta C(t) = C(t) - C^* \quad (6)$$

where C^* is the equilibrium concentration (i.e. the solubility of the solid compound which crystallizes) and $C(t)$ is the actual solute concentration.

The growth of crystals from solution is a complex process which roughly speaking corresponds to the transport of identical dissolved atoms, molecules, ions, complex units, etc, to the solid surface; followed by their ordered integration into the crystal lattice. The crystal growth rate is usually defined as the rate at which a specific or an average characteristic size of the solid particle increases. Despite its lack of physical meaning, the following simplified kinetic empirical law is often used:

$$G_o(t) = \frac{dL}{dt} = k_g(C(t) - C^*(t))^i = k_g \Delta C(t)^i \quad (7)$$

where index *o* will refer in the following to the growth rate in pure solvent.

In eq.(7), exponent i depends on the involved growth mechanism(s). In practice, consistently with "standard" theoretical models, most published values of i are given between 1 and 2.

2. MODELING THE CRYSTAL GROWTH RATE IN THE PRESENCE OF IMPURITIES.

2.1 Effect of the adsorption of impurities on the crystal growth rate.

When compared to the growth of crystals in pure solvent, the time-averaged advancement velocity of a step in impure media can be hindered by the adsorption of impurity species on the growing crystal surface. As schematically shown in Fig. 1, during the step advancement kink sites can be blocked by foreign species that cannot easily incorporate in the crystal lattice. To allow further crystal growth, the growth-step has to circumvent the adsorbed impurity, which obviously reduces the overall growth rate. Several models describing such "pinning mechanism" were early described in the literature (Cabrera & Vermilyea, 1958) and many convincing experimental observations of the pinning mechanism were reported in the literature, notably thanks to the use of advanced imaging techniques such as AFM (Atomic Force Microscopy, see e.g. Land et al., 1999 ; Jiang et al. 2003.; Thomas et al., 2004 ; Geng et al. 2005). An example of impurity unit (Black dot) adsorbed on growth steps of semi-conducting films is displayed in Figure 1b.

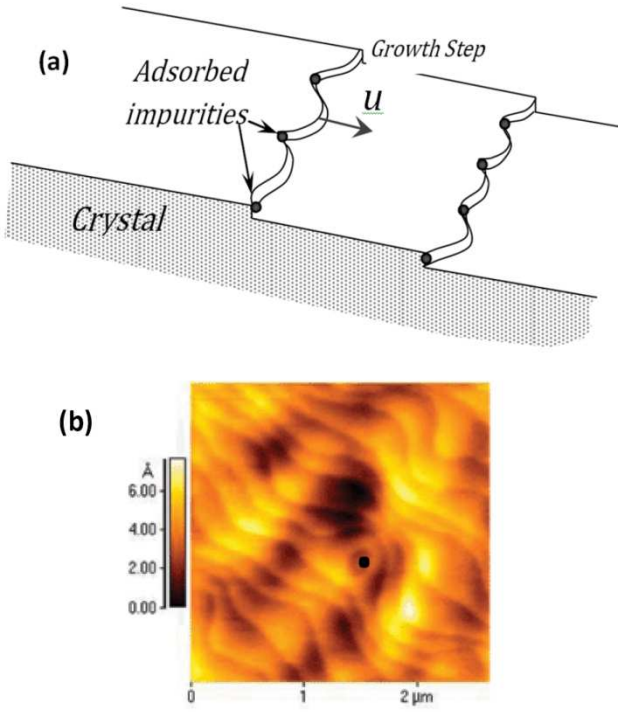

***Figure 1. (a) Adsorption of impurities at kink sites of growing steps after* Kubota (2001) .**

(b) AFM image showing the pinning effect, after Tirado-Mejíast et al., 2006.

Kubota-Mullin's model (1995) was proposed to describe the pinning mechanism through the following ratio Γ between the step velocities in pure (u_0) and impure (u) solvents :

$$\Gamma = \frac{u}{u_0} = 1 - \left[\frac{\gamma a}{kT\sigma L}\right]\theta = 1 - \alpha\theta^* \quad (8)$$

where γ is the edge free energy, a is the size of the growth unit, T is the absolute temperature, k is the Boltzmann constant and $\theta*$ is the steady-state coverage fraction of active growing crystal surface by adsorbed impurities. The notion of step velocity is roughly represented in Figure 1a and one generally assume that $G \propto u$.

The overall parameter α is the effectiveness factor quantifying the efficiency of the impurity specie in hindering the crystal growth. It is very important to notice that α does not only depend on properties of the involved solid, but also on supersaturation. Several approaches can be used to compute the equilibrium coverage $\theta*$. In Kubota-Mullin's Model (Kubota & Mullin, 1995; Kubota et al., 1997), the equilibrium coverage of the growing surface is estimated thanks to Langmuir adsorption theory:

$$\theta^* = K C_i / (1 + K C_i) \quad (9)$$

where K is the Langmuir adsorption constant and C_i is the concentration of impurity.

Even though the adsorption process is often regarded as instantaneous (i.e., the steady-state coverage $\theta*$ is reached instantaneously), it was shown that the dynamics of the adsorption of impurity species on the crystal surface cannot always be neglected. This is the reason why, as a first phenomenological approximation, the transient behavior of the coverage process (i.e. the time variations of θ) was suggested by Kubota (2001) to obey the following first-order dynamics where τ is the time constant of the coverage process:

$$\theta = \theta^* [1 - \exp(-t/\tau)] \quad (10)$$

2.2 General expression of the PBEs accounting for the adsorption of impurities.

Assuming that the crystal growth rate is proportional to the step velocity (i.e. $G/G_o \approx \Gamma$) it finally turns out that *G* depends on both time and supersaturation. Combining expressions (7) to (10) leads to the following expression where ν is the time at which the crystal surface is set in contact with the impure liquid phase. In the industrial practice, impurities might be introduced fortuitously in the mother liquor or, more likely, as undesired products of upstream secondary reactions. In this latter case, the impurities are present from the beginning of the crystallization process so that one can assume that the nucleation events (i.e. primary homogeneous or heterogeneous and further secondary nucleation) occur in the presence of impurities. This is the reason why, in the sequel, the time ν is supposed to coincide with the nucleation time. As an example, the following growth rate expression is considered:

$$\begin{aligned} G(t) &= G_0(t)\left(1-\alpha\frac{KC_i}{1+KC_i}\left[1-exp\left(-\frac{(t-\nu)}{\tau}\right)\right]\right) \\ &= k_g\Delta C(t)^i\left(1-\alpha\frac{KC_i}{1+KC_i}\left[1-exp\left(-\frac{(t-\nu)}{\tau}\right)\right]\right) \end{aligned} \tag{11}$$

Applying the impurity adsorption model to Eq. (1) is not straightforward as it increases the dimension of the problem: the time (*t-ν*) spent by the crystals in contact with impurities should now be accounted for. Even though they are exposed to the same supersaturation, two crystals taken at a given time t do not exhibit the same growth rate *G*. This is why we now introduce a population density function ϕ depending on the "classical" variables, L and t, as well as ν, the time of nucleation of a given particle:

$$\begin{cases} \dfrac{\partial\phi(L,t,\nu)}{\partial t}+G(t,\nu)\dfrac{\partial\phi(L,t,\nu)}{\partial L}=0 & (12) \\ & (13) \\ \phi(L,0,\nu)=0 & (14) \\ \phi(0,t,\nu)=\dfrac{R_N(t)}{G(t,\nu)}\delta(t-\nu) & \end{cases}$$

The standard definition of the crystal size distribution can still be retrieved as:

$$\psi(L,t)=\int_0^\infty\phi(L,t,\nu)d\nu=\int_0^t\phi(L,t,\nu)d\nu \tag{15}$$

3. A METHOD OF CHARACTERISTICS FOR SOLVING POPULATION BALANCE EQUATIONS ACCOUNTING FOR IMPURITY EFFECTS.

A simple method of characteristics for the resolution of the PBE without agglomeration and breakage is now presented, first in the "standard" case corresponding to mono-dimensional crystals generated and grown in pure solvent; and second in the case when the impurity adsorption depends on time.

3.1 A method of characteristics for monodimensional PBEs without impurities.

As already mentioned supersaturation is the driving force of crystallization and computing σ requires computing the time-variations of C(t) during the crystallization process. Actually, the decrease of solute concentration *C(t)* is caused by the generation of crystals: the molecules of solute initially present in the liquid phase are transferred through crystallization to the dispersed solid phase. The total amount of solid is therefore given by the total volume of particles computed through the integration of the whole CSD:

$$C_s(t) = \frac{\rho_s \varphi_p}{M_s} \int_{L^*}^{\infty} \psi(L,t) L^3 dL \cong \frac{\rho_s \varphi_p}{M_s} \int_{0}^{\infty} \psi(L,t) L^3 dL \qquad (16)$$

where ρ_s (kg/m^3) and M_s are the density and the molecular weight of the solid compound, φ_p is a volumetric particle shape factor (equal to π/6 in the "ideal" case of spherical crystals.)

An elementary mass balance of the solute allows computing at each time the evolutions of *C(t)* and consequently yields σ(t) through Eq. (4), provided that experimental data about the solubility curve *C*(T)* are available. Now, in the case of unseeded crystallization process, the PBE system (1-3) is expressed as follows where the growth rate is a complex function of physical and kinetic variables depending on σ and, through the indirect size-dependency of the solute concentration *C(t)*, on the current size distribution:

$$\begin{cases} \dfrac{\psi(L,t)}{\partial t} + G(t)\dfrac{\partial \psi(L,t)}{\partial L} = 0 & (17) \\ \psi(L,0) = 0 & (18) \\ \psi(0,t) = \dfrac{R_N(t)}{G(t)} & (19) \end{cases}$$

During the crystallization process the suspension is kept in supersaturated conditions. One can therefore write that $\sigma > 0$ and the following condition is always fulfilled:

$$\forall t \in \mathbb{R}^+, \forall\, \nu \in [0, t\,], \quad G(t) > 0 \tag{20}$$

Now, the following characteristic curve is considered to describe the size population of particles nucleated at time ν:

$$\forall t \in \mathbb{R}^+, \ \ \forall\, \nu \in [0, t\,] \ \ , \quad \tilde{L}_\nu(t) = \int_\nu^t G(t')dt' \tag{21}$$

As depicted in Figure 2, the CSD along a given characteristic curve is defined as follows:

$$\tilde{\psi}_\nu(t) = \psi\big(\tilde{L}_\nu(t), t\big),$$

so that one can write:

$$\begin{aligned} \frac{d\tilde{\psi}_\nu(t)}{dt} &= \frac{\partial \psi\big(\tilde{L}_\nu(t), t\big)}{\partial t} + \frac{\partial \tilde{L}_\nu(t,\nu)}{\partial t}\ \frac{\partial \psi\big(\tilde{L}_\nu(t), t\big)}{\partial L} \\ &= \frac{\partial \psi\big(\tilde{L}_\nu(t), t\big)}{\partial t} + G(t,\nu)\ \ \frac{\partial \psi\big(\tilde{L}_\nu(t), t\big)}{\partial L} \\ \frac{d\tilde{\psi}_\nu(t)}{dt} &= 0 \end{aligned} \tag{22}$$

It therefore turns out that $\tilde{\psi}_\nu$ does not depend on *t*, which implies that the solution of Eq. (17) is fully determined by the boundary condition (19) and the resolution of (21) describing the time evolutions of the characteristic curves:

$$\forall t \in \mathbb{R}^+, \ \ \forall\, \nu \in [0, t\,] \ \ ,$$

$$\psi\big(\tilde{L}_\nu(t), t\big) = \tilde{\psi}_\nu(t) = \tilde{\psi}_\nu(\nu) = \psi(0, \nu) \tag{23}$$

$$\psi\big(\tilde{L}_\nu(t), t\big) = \frac{R_N(\nu)}{G(\nu)} \tag{24}$$

Now, let us show that eq. (24) allows determining the CSD for every time and size, i.e. every point (*L,t*) in the phase space can be represented thanks to Eq.(21). To this effect, the following application is considered:

,

, is clearly continuous and , —

which, given Eq. (20), shows that λ_t is strictly decreasing and therefore invertible from [0,*t*] to [0,]. It follows that the characteristic curves do not exhibit shock or rarefaction.

A means of computing the distribution density function is therefore given by:

, ,

(25)

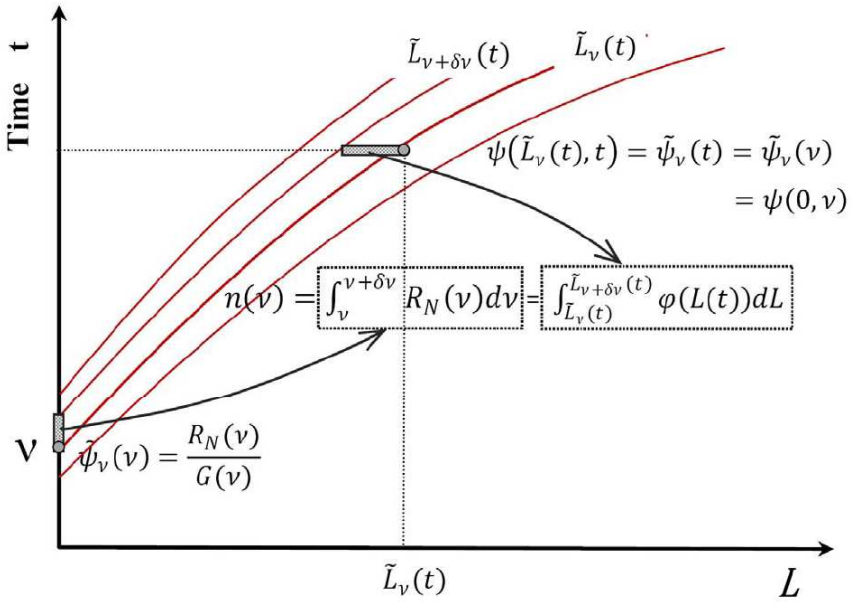

Figure 2. Schematic representation of the coupling between the numbers of particles nucleated at time ν and the overall distribution at time t.

3.2 Semi-discretization of the size population density function.

Considering successive sampling times, the time variable ν is discretized as follows:

, ,

$$\Psi_{\mathrm{i}}(\mathrm{t}) = \int_{\mathrm{L_i(t)}}^{\mathrm{L_{i-1}(t)}} \psi(L,t)dL \tag{26}$$

From Eq.(24), and setting the following change of coordinates:

$$\begin{cases} \nu = \lambda_t^{-1}(L) \\ L = \tilde{L}_\nu(t), \qquad \dfrac{dL}{d\nu} = -G(\nu) \end{cases} \tag{27}$$

we get: $\Psi_{\mathrm{i}}(\mathrm{t}) = \int_{\mathrm{L_i(t)}}^{\mathrm{L_{i-1}(t)}} \psi(L,t)dL = \int_{\nu_{\mathrm{i-1}}}^{\nu_{\mathrm{i}}} \psi\big(\tilde{L}_\nu(t),t\big)G(\nu)d\nu = \int_{\nu_{\mathrm{i-1}}}^{\nu_{\mathrm{i}}} R_N(\nu)d\nu$ (28)

As illustrated in Fig.2, it finally turns out that integrating ψ in size between L_i (t) and L_{i-1} (t), at a given time *t,* amounts to integrating ψ in ν between $\nu_{\mathrm{i-1}}$ and ν_{i}, for a given size, and that the result of this integration does not depend on time t.

Consequently, to solve the system (17-19), one simply has to solve the following two systems coupled by the integral operator *G*. In order not to make the notation heavier, the latter will still be referred to as *G* after discretization:

$$\begin{cases} \dfrac{dL_i}{dt}(t) = G(t) \\ L_i(\nu_i) = 0 \end{cases} ; \begin{cases} \dfrac{d\Psi_i}{dt}(t) = 0 \\ \Psi_i(\nu_i) = \int_{\nu_{i-1}}^{\nu_i} R_N(\nu)\, d\nu \end{cases} \tag{29}$$

3.3 Time-discretization.

Any time-discretization scheme can be used to solve jointly the two systems (29). As an example, *t* might be discretized in the same way as ν (i.e. the same sampling interval dt is used to scan t and ν), which leads to the following simple numerical scheme:

$k = 0$;
while $t_k < t_{end}$ ***do***

> ***for*** $i = 1, k-1$ ***do***
> $L_i(t_k) = L_i(t_{k-1}) + \int_{t_{k-1}}^{t_k} G\Psi(t)dt$;
> ***end***
>
> $L_k(t_k) = 0$;
> $\Psi_{\mathrm{k}}(t) = \int_{t_{k-1}}^{t_k} R_N(\nu)d\nu$;
> $k = k + 1$;

end

3.4 A method of characteristics for monodimensional PBEs accounting for impurity effects.

In order to account for the distribution of growth rates resulting from the adsorption of impurities, the general system (12-14) is now considered. As explained above, the growth rate integral operator G is a complex function of physical and kinetic variables depending on time and, through the indirect size-dependency of the solute concentration, on the whole current size distribution:

$$G(t,\nu) = f\left(t,\nu\,,C^*,m_s \propto \int_0^\infty \phi(L',t,\nu)L'^3\,(t)dL'\right) \tag{30}$$

where m_S is the total mass of crystallized solid.

The nucleation time of every crystal is introduced in Eq. (30) because, as explained in Part 2, the growth rate G depends now on the time spent by the growing crystal in the presence of adsorbing impurities. Now, let us consider characteristic curves defined as follows:

$$\forall t \in \mathbb{R}^+,\ \ \forall\,(\nu,\mu) \in [0,t\,]^2, \qquad \tilde{L}_\mu(t,\nu) = \int_\mu^t G(t',\nu)dt' \tag{31}$$

The distribution along a given characteristic curve is noted:

$\tilde{\phi}_\mu(t) = \phi\big(\tilde{L}_\mu(t,\nu),t,\nu\big)$ and one can write:

$$\begin{aligned}\frac{\partial\tilde{\phi}_\mu(t,\nu)}{\partial t} &= \frac{\partial\phi\big(\tilde{L}_\mu(t,\nu),t,\nu\big)}{\partial t} + \frac{\partial\tilde{L}_\mu(t,\nu)}{\partial t}\ \frac{\partial\phi\big(\tilde{L}_\mu(t,\nu),t,\nu\big)}{\partial L} \\ &= \frac{\partial\phi\big(\tilde{L}_\mu(t,\nu),t,\nu\big)}{\partial t} + G(t,\nu)\ \frac{\partial\phi\big(\tilde{L}_\mu(t,\nu),t,\nu\big)}{\partial L}\end{aligned} \tag{32}$$

$$\frac{\partial\tilde{\phi}_\mu(t,\nu)}{\partial t} = 0 \tag{33}$$

It finally turns out that $\tilde{\phi}_\mu(t,\nu)$ does not depend on t, and it can also be concluded that:

$\forall t \in \mathbb{R}^+,\ \ \forall\,(\nu,\mu) \in [0,t\,]^2,$

$$\phi\big(\tilde{L}_\mu(t,\nu),t,\nu\big) = \tilde{\phi}_\mu(t,\nu) = \tilde{\phi}_\mu(\mu,\nu) = \phi(0,\mu,\nu) \tag{34}$$

$$\phi\big(\tilde{L}_\mu(t,\nu),t,\nu\big) = \delta(\mu-\nu)\frac{R_N(\mu)}{G(\mu,\nu)} \tag{35}$$

3.5 Semi-discretization of the size population density function taking the nucleation time into account.

The time variable μ is discretized considering successive sampling times:

$\mu \in \{\mu_i, i \in \mathbb{N}\}$, and one can define the following distribution function:

$\forall t \in \mathbb{R}^+, \forall\, \nu \in [0, t\,]$

$$L_i(t) = \tilde{L}_{\mu_i}(t, \nu)$$

$$\Phi_{\mathrm{i}}(\mathrm{t}, \nu) = \int_{\mathrm{L_i(t,\nu)}}^{\mathrm{L_{i-1}(t,\nu)}} \phi(L, t, \nu) dL$$

$$\Psi_{\mathrm{i}}(\mathrm{t}) = \int_0^{\mathrm{t}} \Phi_i(t, \nu) d\nu \tag{36}$$

Using Eq.(32) and setting:

$$\begin{cases} \mu = \lambda_{t,\nu}^{-1}(L) \\ L = \tilde{L}_{\mu}(t, \nu), \qquad \dfrac{dL}{d\mu}(\mu) = -G(\mu, \nu) \end{cases} \tag{37}$$

$$\text{yields:} \quad \Phi_{\mathrm{i}}(\mathrm{t}, \nu) = \int_{\mathrm{L_i(t,\nu)}}^{\mathrm{L_{i-1}(t,\nu)}} \phi(L, t, \nu) dL \tag{38}$$

$$= \int_{\mu_{\mathrm{i-1}}}^{\mu_{\mathrm{i}}} \phi\big(\tilde{L}_{\mu}(t, \nu), t, \nu\big) G(\mu, \nu) d\mu \tag{39}$$

$$= \int_{\mu_{\mathrm{i-1}}}^{\mu_{\mathrm{i}}} \delta(\mu - \nu)\, R_N(\mu)\, d\mu \tag{40}$$

$$= \begin{cases} R_N(\nu) & if\ \nu \in [\mu_{i-1}\,; \mu_i] \\ 0 & \text{otherwise} \end{cases} \tag{41}$$

It follows that:

$$\Psi_{\mathrm{i}}(\mathrm{t}) = \int_0^{\mathrm{t}} \Phi_i(t, \nu) d\nu = \int_{\mu_{\mathrm{i-1}}}^{\mu_{\mathrm{i}}} R_N(\nu) d\nu \tag{42}$$

The following two systems are thus obtained which are coupled by the integral operator *G.*

$$G(t) = f\left(t, \mu_i, C^*,\ C_s \propto m_s \propto \sum_i \Psi_i(\mu_i)\, L_i^3(t)\right) \tag{43}$$

$$\begin{cases} \frac{dL_i}{dt}(t) = G(t) \\ L_i(\mu_i) = 0 \end{cases} ; \begin{cases} \frac{d\Psi_i}{dt}(t) = 0 & (44) \\ \Psi_i(\mu_i) = \int_{\mu_{i-1}}^{\mu_i} R_N(\mu)\, d\mu & (45) \end{cases}$$

The principle of the numerical scheme is the same as explained in Part 3.3 and in Figure (2).

4. APPLICATION TO THE SIMULATION OF THE CRYSTALLIZATION OF CITRIC ACID IN THE PRESENCE OF IMPURITIES.

4.1 Effects of impurities on the development of isothermal crystallizations.

In order to illustrate the resolution method, the crystallization of citric acid monohydrate is simulated using kinetic data related to the crystallization of citric acid in water. These data previously published by Févotte et al. (2007) outline clearly the major role played by secondary nucleation mechanisms in the development of the crystallization of citric acid. In the absence of reported experimental studies dealing with impure media, the parameters of Kubota-Mullin's model are set arbitrarily in order to compare the features of crystallization operations performed with and without impurities. The latter data do not correspond to any existing impurity specie that would impair the crystallization of citric acid; they were simply set to reproduce the kinetic features of systems for which, according to Eq.(8), supersaturation thresholds can be observed at the end of the batch process. It is important to notice that in the following no effect of impurities on the rate of nucleation is assumed to occur, even though such assumption is probably unrealistic. Actually, published data about nucleation in the presence of impurities is really lacking and the goal here is rather to show the usefulness of the resolution method and to analyze possible effects of the adsorption of impurities on the development of the crystallization process, than to investigate real solute/solvent/impurity systems.

Isothermal desupersaturation crystallization operations were simulated at 15°C. In order to initiate the crystallization in the supersaturated zone (i.e. $C_{init.}$ >C* at 15°C) a seed mass of 10 kg is supposed to be introduced in a pilot-scale crystallizer fed with a supersaturated citric acid solution containing 1 m^3 of water. The initial dissolved citric acid concentration is C_{init} = 1.825 kg anhydrous CA/kg water. The algorithm presented in Part 3 was applied to

system (11-15) after setting the parameters presented in Tables (1) and (2). As one can see in Figure 3, the computed CSD is smooth and does not exhibit any oscillatory behavior, even when coarse time intervals are used for the numerical simulation (see Part 4.2).

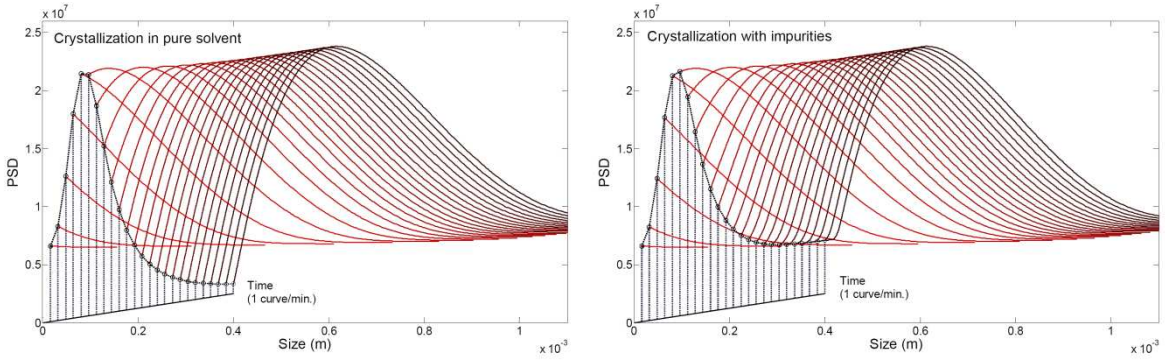

Figure 3. Simulation of seeded isothermal crystallization of citric acid monohydrate in pure water at 15°C: Time variations of the CSD (Number of Particles.$L^{-1}.s^{-1}$). The kinetic parameters are given in Tables 1 and 2. (a) Crystallization performed in pure water. (b) crystallization performed with 0.01 kg.m^{-3} impurities and unsteady-state adsorption (τ=500 s)

After seeding the number of particles increases due to secondary nucleation, and the initial supersaturation is consumed through the growth of crystals, as displayed in Fig. 4d and a. Despite the adsorption of impurity species at the crystal surfaces, the impurity concentration C_i is assumed to remain constant during the crystallization (i.e. the amount of adsorbed molecules is assumed negligible with respect to the dissolved impurities.)

Table 2 shows the parameters used for comparative simulations aiming at analyzing the effect of the concentration C_i on the development of isothermal batch crystallizations. Typical results are displayed in Figure 4 to illustrate the main features of the effects of impurities. As a reference, simulation n°1 corresponds to the crystallization of monohydrate citric acid in pure water, the operating and modeling conditions are the same as previously (See Table 1). Concerning the following simulations the presence of impurities has a clear impact on the development of the CSD and yields, in the average, smaller particles than the ones obtained in pure solvent. In particular, as shown in Figure 4b, the particles obtained at the end of the crystallization process in impure water (Run 4) are about 25% smaller than in pure water (see also Fig.5).

It is worth noting that, as expected, the supersaturation reaches a constant asymptotic value at the end of batch processes with impurities (e.g. σ_{lim}=0.05 for simulation n°4), while less than 1% supersaturation remains after 1500 s during Run 1. Such value of σ_{lim} corresponds to the final threshold supersaturation expected from Kubota-Mullin's model for α>1.

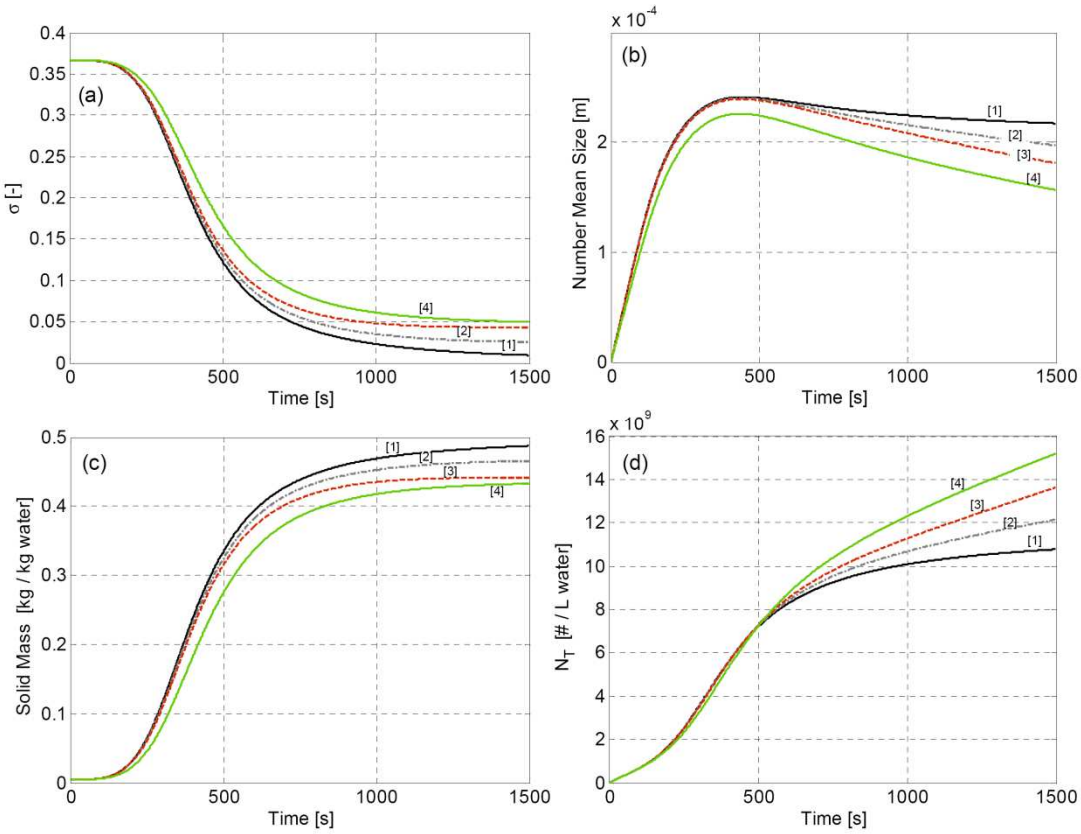

Figure 4. Simulation of seeded isothermal crystallization of citric acid monohydrate in pure water (curve 1) and with the presence of impurities, at 15°C. (a) Desupersaturation profile. (b) Time evolution of the number average crystal size (c) Generation of total crystallized solid during time in kg/L. (d) Time variations of the overall number of crystals in nb/L.

Legend : Run 1 (continuous), 2 (dashed), 3 (dashed-dotted), 4 (dotted), Indices 1 to 4 refer to the parameters in Table 2.

Figure 3 shows the time evolution of the simulated CSDs without (Run 1) and with unsteady-state adsorption of impurities (Run 3). The CSDs are significantly modified by the presence of impurities and the main effect of impurities appears to be the significant generation of fines during the whole batch process, especially at the end where almost no

fines are generated in pure solvent (see final curves in Fig. 4a) while more than 5 10^6 particles/$L^{-1}.s^{-1}$ are generated in the presence of impurities during Run 3. Such amount of fines is likely to exert a detrimental effect on the solid properties (e.g. downstream unit operations like filtration can be made difficult by excessive amounts of fines). It should also be noticed that the bad effects of impurities are damped when the adsorption process is not instantaneous (curves 3 compared with curve 4 in Fig. 4.) With identical impurity concentration it is clear that the dynamic features represented by the overall time constant τ soften the deterioration of the CSD, as well as the reduction of the solid production. However, it is important to remind that the simulations are based on the assumption that the nucleation process remains unaffected by the presence of impurities; the availability of data describing the sensitivity of the nucleation process to impurities might therefore significantly change the main trends observed concerning the effects of impurities on the CSD variations. As outlined in Part 1.2 the final level of supersaturation remains higher when impurities are present in the crystallizing solution, due to the pinning mechanism. As during the present simulation no impurity effect is assumed to affect the secondary nucleation of new citric acid particles, higher levels of supersaturation lead to much a higher overall number of particles (Fig.4d) while, due to growth rate reductions and to the final supersaturation threshold outlined previously, the overall production of solid is clearly reduced. Figure 4c shows that only 86% of the expected solid is obtained at the end of the batch process performed in the presence of impurities (0.5 kg/L of crystals is expected from the values of C_{init} and C*, while only 0.43 kg/L is obtained).

Due to the resolution algorithm, the results presented in Figure 3 might appear as rather misleading because the displayed PSDs are not true population density functions: according to the method presented above every point of a given curve represents the number of particles in the size interval [L, L+ G.dt], where dt is the constant sampling time. It is clear that such size interval is large at the beginning of the crystallization process; while it is small at the end (i.e. G is much smaller at the end). Consequently, the distribution of small particles is under-represented by the curve in Fig. 3. This is the reason why the results were recomputed in terms of normalized size distribution histograms and presented in Fig. 5. The increase of the amount of fines is clearly shown by the final number distribution histogram in Fig. 5a while the reduction of the size of bigger particles is outlined by the weight distribution displayed in Fig. 5b.

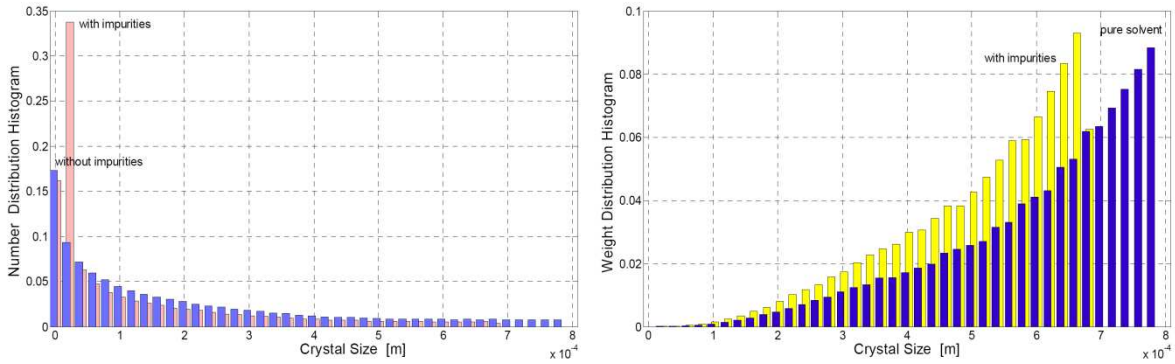

Figure 5. Number and weight particle size distribution histograms obtained at the end of crystallization operations performed without (Run 1) and with impurities (Run 3). Figure 6. Logarithmic plot of the relationship $\Delta_{max}=f(dt)$, the reference simulation was computed with dt=0.005 s

4.2 Some comments on the convergence of the numerical method.

In order to evaluate the convergence of the method as a function of the discretization time-step *dt*, the same simulation was performed with different values of *dt*. Unfortunately, due to the lack of analytical solution, no exact reference simulation is available here, this is why the time-step *dt*=0.005 s was arbitrarily set as a reference allowing to compare the convergence of the solution for increasing time-steps. The "simulation error" was then estimated as follows:

$$\varepsilon_i(\nu) = \frac{\int_0^\nu \mathcal{N}_{ref}(t)dt - \int_0^\nu \mathcal{N}_i(t)dt}{\int_0^\nu \mathcal{N}_{ref}(t)dt}, \qquad \text{for } \nu \in [0, 3000] \tag{46}$$

where $\mathcal{N}_i(t)$ is the computed number of crystals generated between time *t* and *t+dt*, index *i* refers to the simulation under consideration (i.e. performed with a given value of the time step dt) and index 'ref ' refers to the simulation performed with as small as possible time increment dt.

It is clear that the relative error on the computed CSD increases with the time-step. For example, when the time-step increases from 0.02 to 0.05 s, the maximum discrepancy between the 2 cumulative distributions is equal to 10^{-4} (at time t=300 s) which, however, remains quite acceptable. Figure 6 shows a log-log plot of the numerical error in the

cumulative CSD, as a function of the time step. The reference calculation was performed with dt=0.005 s, and the error is computed using the infinite norm. The plot shows that the method presents a convergence order of 1, which is probably mostly limited by the order of the numerical integration formulas used in the scheme to compute Eq.(21).

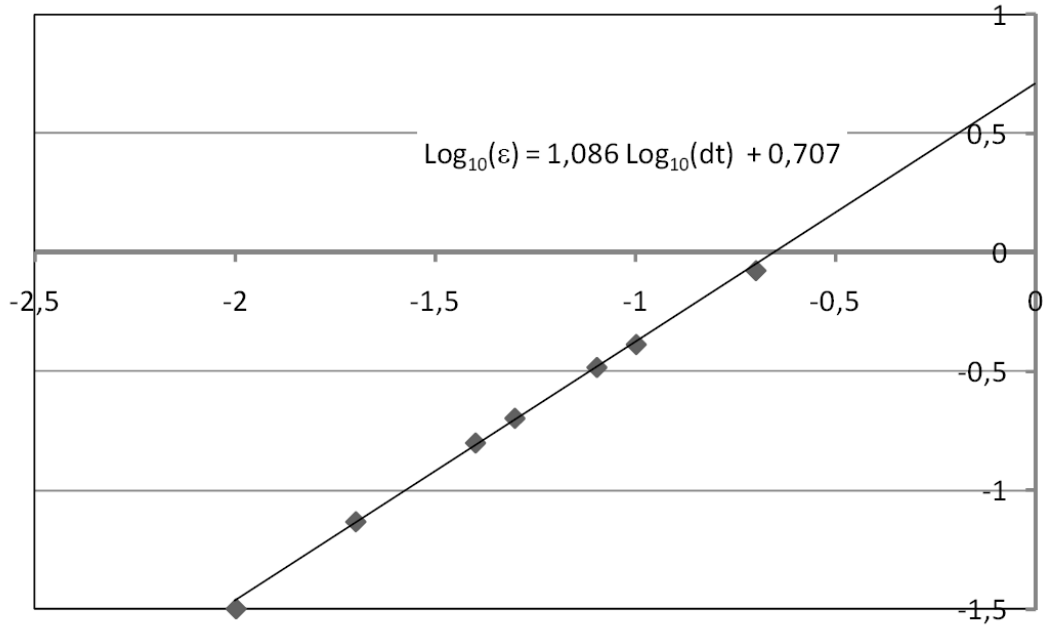

Figure 6. Logarithmic plot of the relationship $\varepsilon_{max}=f(dt)$, the reference simulation was computed with dt=0.005 s

6. CONCLUSIONS

A simple method of characteristics for the resolution of population balance equations applied to crystallization processes without agglomeration and breakage was developed and evaluated through the dynamic simulation of the crystallization of citric acid in water. The method is intended to allow representing growth rate reductions observed during solution crystallizations performed in the presence of industrial impurities.

Indeed, the effect of impurities was shown by Kubota and Mullin (1995) to depend on the time spent by every crystal in the presence of dissolved impurities and consequently, to depend on the "age" of the crystals. Such a particular problem required accounting for an

additional time variable in the expression of the PBEs and finding a way of solving the resulting PBE system.

From a physical viewpoint, the PBE model turns out to be consistent with industrial observations and among other results, the PBE modelling allows representing the reduction of the yield of industrial crystallizations which is generally poorly understood but often attributed to the presence of impurities. The simulations also demonstrate the impact of the unsteady-state behaviour of the adsorption of impurities on the performance of the crystallization process in terms of yield and CSD of the solid product. Such simulations could be applied, for example, to the design of model-based control strategies aiming at improving the productivity of batch crystallizers and/or the quality of crystals generated in impure industrial mother liquors. To the best of our knowledge, such control studies still remain to be undertaken.

As outlined by several authors (e.g. Kumar and Ramkrishna, 1997; Briesen, 2006), despite the apparent simplicity of these two processes, the discretization of crystal nucleation and growth raises numerical diffusion and stability issues which can be attributed to the hyperbolic features of the governing equations (17) to (19). From this latter viewpoint the proposed resolution method offers a very straightforward way of computing nucleation and growth phenomena during crystallization processes.

NOMENCLATURE

C	Solute concentration	kg solute/kg solvent
C*	Solubility concentration	kg solute/kg solvent
C_i	Impurity concentration	$kg.m^{-3}$
C_S	Solid concentration	$kg.m^{-3}$
G	Growth rate	$m.\ s^{-1}$
i	Exponent of the supersaturation dependency of the crystal growth rate	[-]
i_m	Exponent of the dependency of the nucleation	

	rate on the concentration of solid in suspension	[-]
j_m	Exponent of the supersaturation dependency	
	of the nucleation rate	[-]
K	Langmuir's constant	$m^3.\ kg^{-1}$
k_g	Growth rate constant	[-]
K_2	Kinetic nucleation parameter	
L	Particle size	m
N(r,t)	Number of particles at time t in a given subset	$\#.m^{-3}$
R_N	Nucleation rate	$\#.s^{-1}.m^{-3}$
t	Time	s

Greek letters

$\psi(L,t)$	Population density function	$\#.m^{-1}.m^{-3}$
θ	Fraction of coverage of growing crystal surface by adsorbed impurity	
$\theta*$	Fraction of coverage of growing crystal	
	surface by adsorbed impurity at the equilibrium	[-]
ν	Nucleation time	s
τ	Adsorption time constant	s
σ	Supersaturation	[-]

REFERENCES

Briesen, H. (2006) Simulation of crystal size and shape by means of a reduced two-dimensional population balance model. Chem. Engng. Sci.,61, pp. 104-112.

Cabrera, N. ; Vermilyea, D.A., 1958. in Growth and Perfection of Crystals, New York, 393 p.

Chernov, A.A. 2001. Crystal growth science between the centuries. J. Material Sci.: Materials in Electronics, 12, pp. 437-449.

Chernov, A.A., 2004. Notes on interface growth kinetics 50 years after Burton, Cabrera and Frank. Journal of Crystal Growth, 264(4), pp. 499-518.

Chow, A.H.-L., Chow, P.K.K., Zhongshan, W. and Grant, D.J.W., 1985. Modification of acetaminophen crystals: influence of growth in aqueous solutions containing p-acetoxyacetanilide on crystal properties. Int. J. Pharm. 24, pp. 239–258.

Févotte, G., Caillet, A. & Sheibat-Othman, N., 2007. A population balance model of the solution-mediated phase transition of citric acid. AIChE Journal, 53(10), pp. 2578-2589.

Geng, Y.L.; Xu, D.; , Wang, Y.L.; Du, W.; Liu, H.Y.; Zhang, D.H. and Wang, X.Q. 2005. Atomic force microscopy study on surface morphologies of {1 1 0} faces of MnHg(SCN)4 crystals. J. Cryst. Growth, 277, 1-4, pp. 555-559

Jiang, X.N. ; Xu, D. ; Sun, D.L. ; Yuan, D.R.; Zhang, Q.Y. 2003. Atomic force microscopy studies on surface morphologies of CdHg(SCN)4 crystals grown in solutions containing excessive amount of Cd(II) cations. Cryst. Res. Technol. 38, 2, pp. 143 – 149.

Johnson, Douglas S.; Li, Jie Jack (2007) The Art of Drug Synthesis. Wiley-Interscience, 276 p.

Kubota, N. & Mullin, J.W., 1995. A kinetic model for crystal growth from aqueous solution in the presence of impurity. Journal of Crystal Growth, 152(3), pp. 203-208.

Kubota, N. 2001. Effect of Impurities on the Growth Kinetics of Crystals. Cryst. Res. Technol., 36 (8-10), pp.749–769.

Kubota, N., Yokota, M. & Mullin, J.W., 1997. Supersaturation dependence of crystal growth in solutions in the presence of impurity. Journal of Crystal Growth, 182(1-2), 86-94.

Kubota, N., Yokota, M. & Mullin, J.W., 2000. The combined influence of supersaturation and impurity concentration on crystal growth. Journal of Crystal Growth, 212(3-4), pp. 480-488.

Kumar, S. and Ramkrishna, D. (1996a). On the solution of population balance equations by discretization--I. A fixed pivot technique, *Chem. Engng. Sci.,* 51, 8, pp. 1311-1332.

Kumar,S., and Ramkrishna, D. (1996b). On the solution of population balance equations by discretization--II. A moving pivot technique, *Chem. Engng. Sci.,* 51, 8, pp. 1333-1342.

Kumar, S. and Ramkrishna, D. (1997). On the solution of population balance equations by discretization- III. Nucleation, growth and aggregation of particles, *Chem. Engng. Sci*. 52, 24, pp. 4659-4679.

Land, T.A., Martin, T.L., Potapenko, S., Palmore, G.T., De Yoreo, J.J. (1999). Recovery of surfaces from impurity poisoning during crystal growth. *Nature*, 399, pp. 442-445.

Liao, Y. and Lucas, D. 2009. A literature review of theoretical models for drop and bubble breakup in turbulent dispersions. Chem. Eng. Sci., 64, 15, pp. 3389-3406.

Mersmann, A.; B. Braun, B. and Löffelmann, M. 2002. Prediction of crystallization coefficients of the population balance. Chem. Eng. Sci., 57, 20, pp. 4267-4275

Myerson,A. S., 2001. Handbook of Industrial Crystallization. Second ed., Butterworh-Heinemann, 304 p.

Qamar,S.; Warnecke,G. (2007). Numerical solution of population balance equations for nucleation, growth and aggregation processes, *Comp. & Chem. Engng*. 31, pp. 1576-1589.

Raghavan,S. L.; Trividic,A.; Davis,A. F.; Hadgraft,J. 2001. Crystallization of hydrocortisone acetate: influence of polymers. Int. J. Pharm. 212, 2, pp. 213-221.

Ramkrishna, D., 2000. Population Balances: Theory and Applications to Particulate Systems in Engineering, Academic Press.

Ramkrishna, D.; Mahoney, A.W. 2002. Population balance modeling. Promise for the future. Chem. Eng. Sci., 57, 4, pp. 595-606.

Sangwal, K., 1996. Effects of impurities on crystal growth processes. Progress in Crystal Growth and Characterization of Materials, 32(1-3), pp. 3-43.

Sangwal, K., 2002. On the nature of supersaturation barriers observed during the growth of crystals from aqueous solutions containing impurities. Journal of Crystal Growth, 242(1-2), 215-228.

Sangwal, K., 2007. Additives and Crystallization Processes. From Fundamentals to Applications. John Wiley & Sons. 451 p.

Sotowa, K.I., Naito, K., Kano, M., Hasebe, S., Hashimoto, I. (2000). Application of the method of characteristics to crystallizer simulation and comparison with finite difference for controller performance evaluation. *J. of Process Control*, 10, pp. 203-208.

Thomas, T.N., Land, T.A., Martin, T., Casey, W.H., DeYoreo, J.J. (2004). AFM investigation of step kinetics and hillock morphology of the {1 0 0} face of KDP. *J. Crystal Growth,* 260(3-4), pp. 566-579.

Tirado-Mejíast, L.; Ramírez, J.G.; Gómez, M.E.; Ariza-CalderónI, H. 2006. Surface morphology analysis of GaInAsSb films grown by liquid phase epitaxy. Braz. J. Phys. 36, 3b.

Vale, H.M. and T.F. McKenna, T.F. 2005. Modeling particle size distribution in emulsion polymerization reactors. Progress in Polymer Science, 30, 10, pp. 1019-1048.

Wood, W.M.L., 2001. A bad (crystal) habit--and how it was overcome. Powder Technology, 121(1), pp. 53-59.

ACKNOWLEDGEMENTS

We greatly acknowledge the French research agency ANR for the support granted to the project “IPAPI” (Improving the Properties of Active Pharmaceutical Ingredients), ref. 07-BLAN-0183

Table 1. Kinetic equations and parameters used for the simulation of the crystallization of Citric Acid monohydrate.

$$\frac{dL}{dt} = G(t) = k_g.(C(t) - C_m^*(T))^j$$

$$= 7.18\ 10^{-6}.\left(C(t) - C_m^*(T)\right)^{1.58}$$

$$R_N(t) = k_2.C_S(t)^{i_m}.\left(C(t) - C_m^*(T)\right)^{j_m}$$

$$= 1.72\ 10^8.C_S(t)^{0.47}(C(t) - C_m^*(T))^{1.14}$$

where: $R_N(t)$ is the secondary surface nucleation rate of monohydrated citric acid [#.s^{-1}.m^{-3}]

k_2 is a "lumped" kinetic constant for the secondary nucleation of monohydrated citric acid

C_m^* is the solubility in water of monohydrated citric acid (1.35 kg/kg water at 15°C)

i, i_m, j_m are exponents proposed by Févotte et al. (2006)

Parameters of Kubota's-Mullin's adsorption model:

K =5	[m3/kg]
τ =500	[s]
C_i =0.01	[kg/m^3]
$\alpha.\sigma$ = 1	

Table 2. Parameters of Kubota-Mullin's model used for the batch simulations displayed in Figures 4 and 5.

Simulation n°	K $(kg.m^{-3})^{-1}$	C_i $(kg.m^{-3})$	τ (s)
1	-	0	-
2	5	0.005	500
3	5	0.01	500
4	5	0.01	0